Supplementary material to

Dynamic Mathematical Modeling of IL13-induced Signaling in Hodgkin and Primary Mediastinal B-cell Lymphoma Allows Prediction of Therapeutic Targets

Valentina Raia, Marcel Schilling, Martin Böhm, Bettina Hahn, Andreas Kowarsch, Andreas Raue, Carsten Sticht, Sebastian Bohl, Maria Saile, Peter Möller, Norbert Gretz, Jens Timmer, Fabian Theis, Wolf-Dieter Lehmann, Peter Lichter, Ursula Klingmüller

Table of contents

- Supplementary methods p. 1
- Supplementary text p. 5
- Supplementary references p. 28

Supplementary methods

Methods S1. Isolation of human B cells

Primary human B cells were isolated from buffy coats of healthy donors purchased from IKTZ Heidelberg Blood Bank (Heidelberg, Germany). Briefly, buffy coats were diluted 1:3 in RPMI 1640 and stratified on a Ficoll gradient (Biocoll separating solution, Biochrom AG, Berlin, Germany). The obtained mononuclear cells were then labeled with human CD19 MicroBeads (Miltenyi Biotec, Bergisch Gladbach, Germany) and positively selected by magnetic activated cell sorting. The isolation yield was <5 x 10^5 B cells from each buffy coat bag (~60 ml). For immunoblotting experiments ~3-5 x 10^6 cells were needed per time point. Before experiments, these cells were starved for one hour. B-cell purity was verified by staining with phycoerythrine (PE)-coupled anti-CD20 antibody followed by flow cytometry analysis of the sorted cells at a FACSCalibur™ Flow Cytometer (BD Biosciences, San Jose, CA), and proved to be ~90% (see figure below).

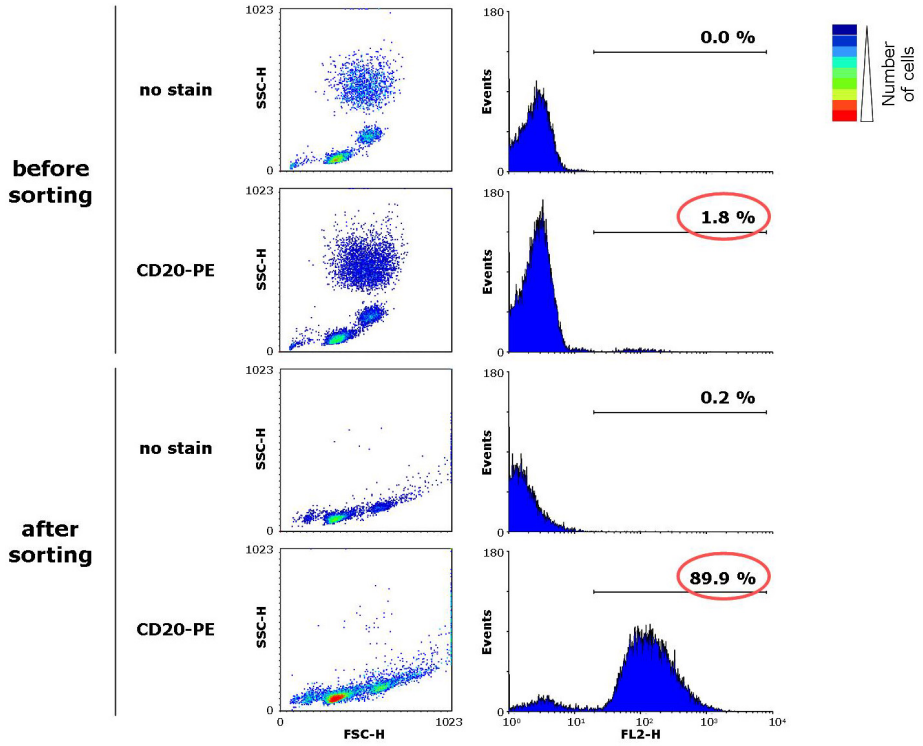

Fig. S1. B-cell purity. Flow cytometry analysis showing the percentage of CD20+ B cells before magnetic activated cell sorting and after sorting. Non-stained cells are shown as negative controls.

Table S2. qRT-PCR reaction scheme (LightCycler® 480) and primer list

Program Name	Pre-Incubation		
Cycles	1	Analysis Mode	None

Target (°C)	Acquisition Mode	Hold (hh:mm:ss)	Ramp Rate (°C/s)
95	None	00:05:00	4.40

Program Name	Amplification		
Cycles	50	Analysis Mode	Quantification

Target (°C)	Acquisition Mode	Hold (hh:mm:ss)	Ramp Rate (°C/s)
95	None	00:00:10	4.40
60	None	00:00:30	2.20
72	Single	00:00:01	4.40

Program Name	Cooling		
Cycles	1	Analysis Mode	None

Target (°C)	Acquisition Mode	Hold (hh:mm:ss)	Ramp Rate (°C/s)
40	None	00:02:00	1.50

Gene symbol	mRNA accession	Forward primer (5'-3')	Reverse primer (5'-3')	UPL_Probe number
HPRT	NM_000194.2	tgaccttgatttattttgcatacc	cgagcaagacgttcagtcct	73
CD274	NM_014143.2	ggcatccaagatacaaactcaa	cagaagttccaatgctggatta	25
CISH	NM_145071.1	agccaagaccttctcctacctt	tggcatcttctgcaggtgt	20
SOCS3	NM_003955.3	agacttcgattcgggacca	aacttgctgtgggtgacca	36

Methods S3. Immunoprecipitations, quantitative immunoblotting, data analysis and recombinant proteins

At the indicated time points, constant amounts of cells were lysed by the addition of 2 X Nonidet P-40 lysis buffer (1). For each sample an immunoprecipitation (IP) was performed with protein lysate, appropriate antibody and Protein A Sepharose™ CL-4B or Protein G Sepharose™ beads (GE Healthcare, Little Chalfont, United Kingdom). Human recombinant proteins (calibrators) (2) were added to the IPs at constant amounts in each sample as controls or as dilution series to determine the number of molecules per cell of the protein of interest. SDS-PAGE and immunoblotting (IB) were performed and analyzed as previously described (3). Chemiluminescent band signals were acquired in non-saturating substrate conditions by a LumiImager (Roche, Mannheim, Germany), an instrument based on a charge-coupled device (CCD)-camera. Chemiluminescent signals were quantified using LumiAnalyst software (Roche). Results from each experiment were normalized by dividing each value with the average of the values corresponding to the lowest IL13 dose. This allowed merging and averaging data from different experiments. When 3 or more values were available for a specific time-point, standard deviation and average were calculated for that time point. Average values of data from the same experiment repetitions were plotted against their standard deviations. A linear regression was performed and the offset and slope were used as absolute and relative error of the corresponding data set, respectively (linear error model).

GST-SHP1 recombinant protein was purchased from Millipore (Billerica, MA). In order to produce the recombinant proteins GST-STAT6, GST-ΔSTAT5, GST-ΔJAK2 and SBP-SOCS3, full length STAT6 cDNAs and partial length STAT5 and JAK2 cDNAs were cloned into pGEX-2T vector (GE Healthcare, Little Chalfont, United Kingdom), while full length SOCS3 was cloned into pSBPEX-2T vector, a pGEX-2T vector where the GST sequence was replaced by the SBP one.

- To generate the pGEX-2T_STAT6 plasmid encoding for GST-STAT6 recombinant protein, STAT6 cDNA was amplified using the primer sequences 5'-atagtttaaacatgtctctgtggggtctg-3' and 5'-

catgaattctcaccaactggggttgg-3' and the PCR fragment was digested with PmeI and EcoRI and cloned into pGEX-2T treated with BamHI (whose protruding end was filled by T4 DNA Polymerase) and EcoRI.

- To generate the pGEX-2T_ΔSTAT5B plasmid encoding for GST-ΔSTAT5 recombinant protein, STAT5B cDNA was amplified using the primer sequences 5'-cgcggatccttcatcatcgagaagcag-3' and 5'-ccggaattctcatgactgtgcgtgaggaa-3' and the PCR fragment was digested with BamHI and EcoRI and cloned into pGEX-2T treated with BamHI and EcoRI.
- To generate the pGEX-2T_ΔJAK2 plasmid encoding for GST-ΔJAK2 recombinant protein, JAK2 cDNA was amplified using the primer sequences 5'-cgcggatccttaatatttaatgaaagtcttgg-3' and 5'-ccggaattcctatactgtcccgcatttgatcc-3' and the PCR fragment was digested with BamHI and EcoRI and cloned into pGEX-2T treated with BamHI and EcoRI.
- To generate the pSBPEX-2T_SOCS3 plasmid encoding for SBP-SOCS3 recombinant protein, SOCS3 cDNA was amplified using the primer sequences 5'-cgggatccatggtcacccacagc-3' and 5'-cggaattccttaaagtggagcatcat-3' and the PCR fragment was digested with BamHI and EcoRI and cloned into pSBPEX-2T treated with BamHI and EcoRI.

All recombinant proteins, including the truncated ones, retained the domain containing the epitope for the binding of the antibody.

Expression plasmids were transformed into competent *E. coli* BL21-CodonPlus (DE3)-RIL cells (Agilent Technologies - Stratagene Products, Waldbronn, Germany) for recombinant proteins expression. Recombinant proteins were purified as described previously (4).

In case of SOCS3 only, streptavidin binding peptide (SBP) beads were used instead of Glutathione-Agarose ones and Biotin (Sigma-Aldrich Chemie Gmbh, Munich, Germany) was used for elution instead of reduced glutathione. Quantification and purity check were performed by SDS-PAGE followed by SimplyBlue™ SafeStain (Invitrogen, Darmstadt, Germany) staining. BSA dilution series in known concentrations were loaded on the same gels, BSA band intensities were measured and a linear regression was calculated and used for estimation of protein concentration of recombinant protein samples. To check the sequence of the cloned vector, 1 μg of DNA was sequenced by MWG-Biotech using the dideoxy-chain termination method (5).

Methods S4. Antibodies

For immunoprecipitations (IP) and immunoblotting (IB) the following antibodies were used: anti-IL4Ra, anti-STAT5 and anti-SHP1 (Santa Cruz Biotechnology, Santa Cruz, CA), anti-STAT6 (R&D Systems, Minneapolis, MN), anti-phospho tyrosine 4G10 for IB only (Millipore, Billerica, MA), anti-JAK2 (Millipore for IP, Millipore or MBL International, Woburn, MA, for IB), anti-SOCS3 (Invitrogen, Darmstadt, Germany, for IP, Abcam, Cambridge, United Kingdom, for IB). IB secondary antibodies were anti-mouse and protein A HRP (GE Healthcare, Little Chalfont, United Kingdom).

	% positive cells		
Antibody	CHO_IL13Ra1	CHO_IL13Ra2	CHO
anti-IL13Ra2	3	94	2
anti-IL13Ra1	89	3	1

Table S4. Specificity of anti-IL13Ra2 antibody demonstrated by flow cytometry. Percentage of positive cells detected by anti-IL13Ra2 in IL13Ra2-transfected Chinese hamster ovary (CHO) cells (CHO_IL13Ra2), in IL13Ra1-transfected CHO cells (CHO_IL13Ra1) and in untransfected CHO cells (CHO). As comparison, the specificity of an anti-IL13Ra1 antibody is also provided.

All antibodies used for flow cytometry analysis were PE-conjugated. Anti-IL4Ra, anti-CD20 and the appropriate isotype controls were from BD Biosciences (San Jose, CA) and anti-IL13Ra2 from Abcam. The anti-IL13Ra2 antibody specifically recognizes IL13Ra2 and not IL13Ra1, as demonstrated upon our request by the manufacturing company (see table above).

Methods S5. Data analysis of gene expression arrays

Samples for gene expression arrays were collected at the following time-points: 0, 0.5, 1, 1.5, 2, 3, 4, 6, 8, 12 hours after IL13 stimulation (http://www.ncbi.nlm.nih.gov/geo/query/acc.cgi?token=nxyxhuauwymsahq&acc=GSE23591). Data were analyzed in two ways. To identify common up-regulated genes, the ~29,000 genes were normalized by quantile normalization for each cell line and ~7,000 unknown genes were excluded from further analysis. The intensity values of all time points for each gene were normalized to 1, where 1 was the average of the values of the two time points 0. After this normalization, genes were selected according to the average of the values measured at time points 0.5 to 2 h and 0.5 to 12 h.

In a second approach, we aimed to identify biological processes induced by IL13 stimulation in the two cell lines. We used the GraDe algorithm, which incorporates prior knowledge in forms of transcriptional regulation, protein-protein interactions or metabolic pathways and matrix factorization methods (6). To apply GraDe, we link all expressed genes along a gene regulatory network derived from the TRANSPATH database (7). By linking genes, we introduce a partial ordering and are able to define an auto-correlation function. Using this framework as constraint to the matrix factorization task, GraDe is able to identify graph-autodecorrelated signals in the time-course microarray data sets. Extracted graph–decorrelated gene expression sources (GES), were labeled from 1 to 10 according to their decreasing eigenvalues. We then selected all genes in the positive submodes by choosing a threshold ≥ 2 as well as all genes in the negative submodes by a threshold ≤ -2, respectively. These sets were subsequently used for GO enrichment analysis using a p-value < 0.05 corrected by the Benjamini Hochberg procedure.

Methods S6. MATLAB modeling tools

PottersWheel 2.0.47
Version of PottersWheel MEX files: 2010-01-21
System: PCWIN
Matlab 7.9.0.529 (R2009b)
Matlab Optimization toolbox available: Version 4.3
Matlab Splines toolbox available: Version 3.3.7
Matlab Statistics toolbox available: Version 7.2
Matlab Symbolic math toolbox available: Version 5.3
CVODES integrator: available.

Supplementary text

Text S7. Model description

In MedB-1 model IL13 binds to Rec and the resulting species IL13_Rec triggers the phosphorylation of JAK2. pJAK2 phosphorylates IL13_Rec that in turn also contributes to the phosphorylation of JAK2. pJAK2 phosphorylates STAT5 and pSTAT5 activates the transcription of target genes (CD274mRNA, SOCS3mRNA). The signal strength depends on Rec_i (receptor recycle), on p_IL13_Rec internalization and degradation and on the negative regulators SHP1, which de-phosphorylates pJAK2 and pSTAT5, as well as SOCS3, which is translated from SOCS3mRNA and inhibits the phosphorylation of JAK2. IL13 can also bind to DecoyR, forming the complex IL13_DecoyR without contributing to JAK2/STAT5 signaling. In the L1236 model SOCS3mRNA, SOCS3 protein, DecoyR and the associated reactions are not present.

Text S8. Model reactions and parameters

MedB-1

Model equations:

Rec	$\dot{x}_1 = - k_1 \cdot u_1 \cdot x_1 \cdot 2.265 - k_5 \cdot x_1 + k_6 \cdot x_2$
Rec_i	$\dot{x}_2 = + k_5 \cdot x_1 - k_6 \cdot x_2$
IL13_Rec	$\dot{x}_3 = + k_1 \cdot u_1 \cdot x_1 \cdot 2.265 - k_2 \cdot x_3 \cdot x_7$
p_IL13_Rec	$\dot{x}_4 = + k_2 \cdot x_3 \cdot x_7 - k_3 \cdot x_4$
p_IL13_Rec_i	$\dot{x}_5 = + k_3 \cdot x_4 - k_4 \cdot x_5$
JAK2	$\dot{x}_6 = - k_7 \cdot x_3 \cdot x_6 / (1 + k_{13} \cdot x_{14}) - k_7 \cdot x_4 \cdot x_6 / (1 + k_{13} \cdot x_{14}) + k_8 \cdot x_7 \cdot x_8$
pJAK2	$\dot{x}_7 = + k_7 \cdot x_3 \cdot x_6 / (1 + k_{13} \cdot x_{14}) + k_7 \cdot x_4 \cdot x_6 / (1 + k_{13} \cdot x_{14}) - k_8 \cdot x_7 \cdot x_8$
SHP1	$\dot{x}_8 = 0$
STAT5	$\dot{x}_9 = - k_9 \cdot x_9 \cdot x_7 + k_{10} \cdot x_{10} \cdot x_8$
pSTAT5	$\dot{x}_{10} = + k_9 \cdot x_9 \cdot x_7 - k_{10} \cdot x_{10} \cdot x_8$
SOCS3mRNA	$\dot{x}_{11} = + x_{10} \cdot k_{11}$
DecoyR	$\dot{x}_{12} = - k_{12} \cdot u_1 \cdot x_{12} \cdot 2.265$
IL13_DecoyR	$\dot{x}_{13} = + k_{12} \cdot u_1 \cdot x_{12} \cdot 2.265$
SOCS3	$\dot{x}_{14} = + x_{11} \cdot k_{14} / (k_{15} + x_{11}) - k_{16} \cdot x_{14}$
CD274mRNA	$\dot{x}_{15} = + x_{10} \cdot k_{17}$

u_1 is the input.

The value 2.265 is a correction factor to convert ng/ml of IL13 into IL13 molecules per cell. This factor is different in the two models because due to different cell size of MedB-1 and L1236 cells, in our experimental setup they were used at different concentrations.

Parameters of MedB-1 model

Dynamic parameters	*Values*
k_1 = Kon_IL13Rec	0.00342
k_2 = Rec_phosphorylation	999.63100
k_3 = pRec_intern	0.15254
k_4 = pRec_degradation	0.17292
k_5 = Rec_intern	0.10335
k_6 = Rec_recycle	0.00136
k_7 = JAK2_phosphorylation	0.15706
k_8 = pJAK2_dephosphorylation	0.00062
k_9 = STAT5_phosphorylation	0.03826
k_{10} = pSTAT5_dephosphorylation	0.00034
k_{11} = SOCS3mRNA_production	0.00216
k_{12} = DecoyR_binding	0.00012
k_{13} = JAK2_p_inhibition	0.01683
k_{14} = SOCS3_translation	11.90860
k_{15} = SOCS3_accumulation	3.70803
k_{16} = SOCS3_degradation	0.04292
k_{17} = CD274mRNA_production	0.00008

Scaling parameters	
k_{18} = Rec_i	113.19400
k_{19} = scale_pJAK2	1.39040
k_{20} = scale_pIL4Ra	1.88700
k_{21} = scale_IL13-cell	5.56750
k_{22} = scale_SOCS3mRNA	17.66990
k_{23} = scale_CD274mRNA	2.48547

Fixed initial concentrations (if not zero)

Species	*Molecules per cell (x 1000)*
Rec:	1.3
JAK2:	2.8
SHP1:	91
STAT5:	165
DecoyR:	0.34

Instead of fixing the non-zero initial concentrations to the measured values, we also tried to estimate these parameters using the measured values as observables in conjunction with the determined standard deviations. The goodness of fit and the estimated parameters were essentially the same for both methods. Thus, we fixed the non-zero initial conditions to keep the number of estimated parameters as small as possible.

Due to setting restrictions on the parameter range (between 1e-9 and 1e+3), the parameter value of Rec_phosphorylation is close to 1000. This indicates that receptor phosphorylation is too fast to be accurately estimated given the time scale of the experimental data.

Note: For MedB-1 model, we used 207 data-points to fit 23 parameters. This high ratio of data points to model parameters prevented over-parameterization.

L1236

Model equations:

Rec	$\dot{x}_1 = - k_1 \cdot u_1 \cdot x_1 \cdot 3.776 - k_5 \cdot x_1 + k_6 \cdot x_2$
Rec_i	$\dot{x}_2 = + k_5 \cdot x_1 - k_6 \cdot x_2$
IL13_Rec	$\dot{x}_3 = + k_1 \cdot u_1 \cdot x_1 \cdot 3.776 - k_2 \cdot x_3 \cdot x_7$
p_IL13_Rec	$\dot{x}_4 = + k_2 \cdot x_3 \cdot x_7 - k_3 \cdot x_4$
p_IL13_Rec_i	$\dot{x}_5 = + k_3 \cdot x_4 - k_4 \cdot x_5$
JAK2	$\dot{x}_6 = - k_7 \cdot x_6 \cdot x_3 - k_7 \cdot x_6 \cdot x_4 + k_8 \cdot x_7 \cdot x_8$
pJAK2	$\dot{x}_7 = + k_7 \cdot x_6 \cdot x_3 + k_7 \cdot x_6 \cdot x_4 - k_8 \cdot x_7 \cdot x_8$
SHP1	$\dot{x}_8 = 0$
STAT5	$\dot{x}_9 = - k_9 \cdot x_9 \cdot x_7 + k_{10} \cdot x_{10} \cdot x_8$
pSTAT5	$\dot{x}_{10} = + k_9 \cdot x_9 \cdot x_7 - k_{10} \cdot x_{10} \cdot x_8$
CD274mRNA	$\dot{x}_{11} = + x_{10} \cdot k_{11}$

u_1 is the input.

The value 3.776 is a correction factor to convert ng/ml IL13 into IL13 molecules per cell. This factor is different in the two models because due to different cell size of MedB-1 and L1236 cells, in our experimental setup they were used at different concentrations.

Parameters of L1236 model

Dynamic parameters	*Values*
k_1 = Kon_IL13Rec	0.00174087
k_2 = Rec_phosphorylation	9.07541
k_3 = pRec_intern	0.324132
k_4 = pRec_degradation	0.417538
k_5 = Rec_intern	0.259686
k_6 = Rec_recycle	0.0039243
k_7 = JAK2_phosphorylation	0.300019
k_8 = pJAK2_dephosphorylation	0.0981611
k_9 = STAT5_phosphorylation	0.00426767
k_{10} = pSTAT5_dephosphorylation	0.0116389
k_{11} = CD274mRNA_production	0.0115928

Scaling parameters	
k_{12} = Rec_i	118.598
k_{13} = scale_pJAK2	0.469837
k_{14} = scale_pIL4Ra	1.80003
k_{15} = scale_IL13-cell	174.727
K_{16} = scale_CD274mRNA	0.110568

Fixed initial concentrations (if not zero)

Species	*Molecules per cell (x 1000)*
Rec:	1.8
JAK2:	24
SHP1:	9.4
STAT5:	209

Instead of fixing the non-zero initial concentrations to the measured values, we also tried to estimate these parameters using the measured values as observables in conjunction with the determined standard deviations. The goodness of fit and the estimated parameters were essentially the same for both methods. Thus, we fixed the non-zero initial conditions to keep the number of estimated parameters as small as possible.

Note: For L1236 model, we used 141 data-points to fit 16 parameters. This high ratio of data points to model parameters prevented over-parameterization.

Figure S9. Constant SHP1 levels over time

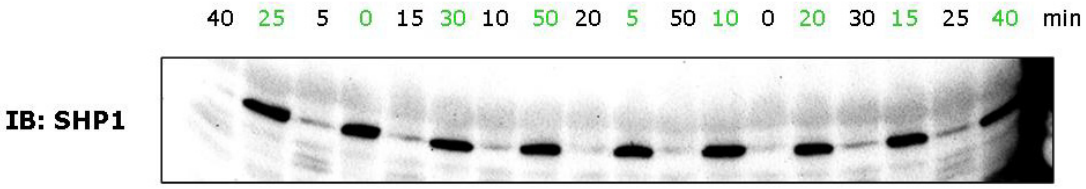

Fig. S9. SHP1 levels are constant over time. Time-course of SHP1 in MedB-1 cells stimulated with 20 ng/ml IL13 (green) and L1236 cells stimulated with 8 ng/ml IL13 (black). Constant amounts of cell lysate were loaded in each gel lane and SHP1 was detected by quantitative immunoblotting. Band chemiluminescent signal quantification was performed with LumiAnalyst software.

Figure S10. STAT5-SHP1 interaction

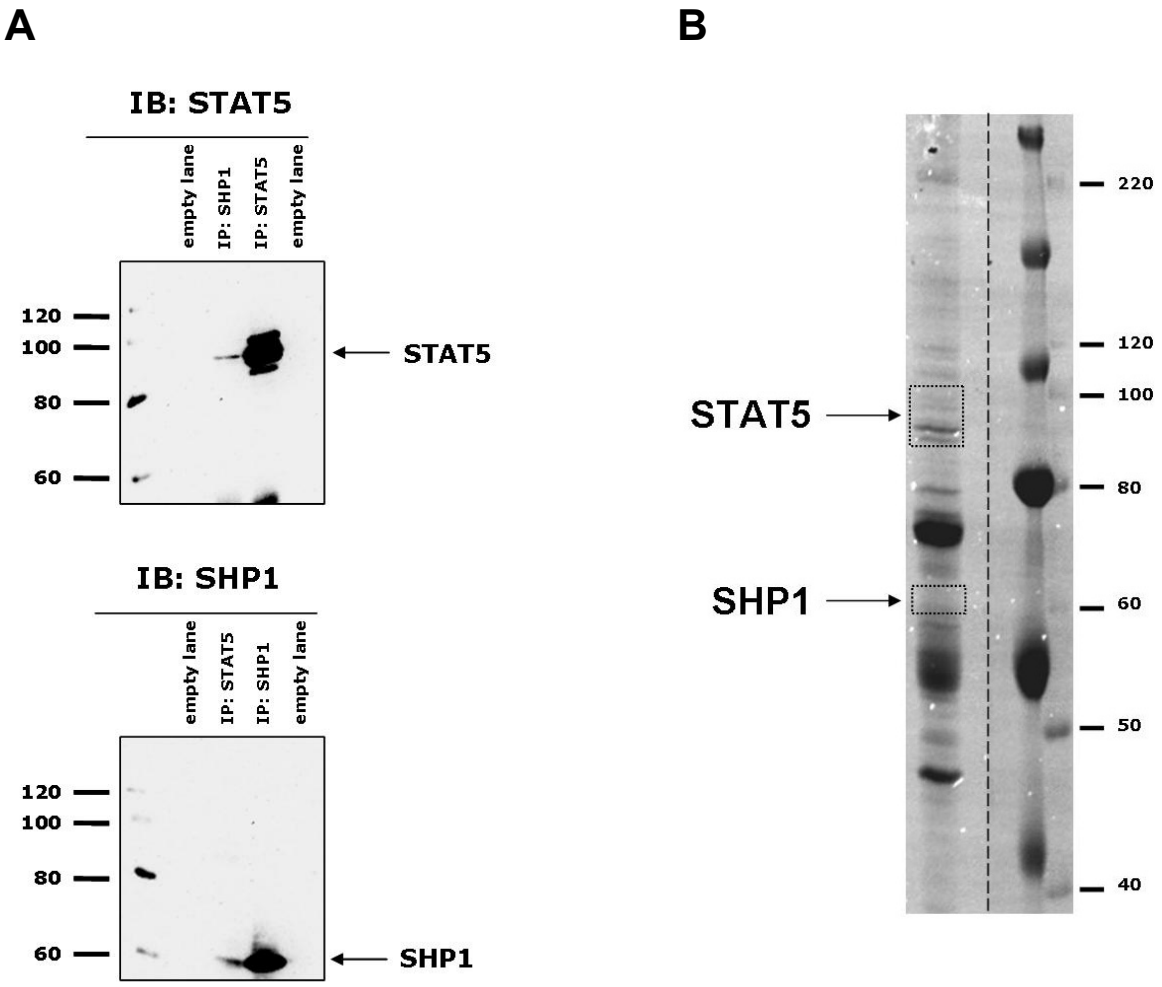

C

```
  1 mvrwfhrdls gldaetllkg rgvhgsflar psrknqgdfs lsvrvgdqvt
 51 hiriqnsgdf ydlyggekfa tltelveyyt qqqgvlqdrd gtiihlkypl
101 ncsdptserw yhghmsggqa etllqakgep wtflvresls qpgdfvlsvl
151 sdqpkagpgs plrvthikvm ceggrytvgg letfdsltdl vehfkktgie
201 easgafvylr qpyyatrvna adienrvlel nkkqesedta kagfweefes
251 lqkqevknlh qrlegqrpen kgknryknil pfdhsrvilq grdsnipgsd
301 yinanyiknq llgpdenakt yiasqgclea tvndfwqmaw qensrvivmt
351 trevekgrnk cvpywpevgm qraygpysvt ncgehdttey klrtlqvspl
401 dngdlireiw hyqylswpdh gvpsepggvl sfldqinqrq eslphagpii
451 vhcsagigrt gtiividmlm enistkgldc didiqktiqm vraqrsgmvq
501 teaqykfiyv aiaqfiettk kklevlqsqk gqeseygnit yppamknaha
551 kasrtsskhk edvyenlhtk nkreekvkkq rsadkekskg slkrk
```

Fig. S10. STAT5 and SHP1 interact with each other. **A**, Immunoblots showing Co-IP of STAT5 with SHP1 and of SHP1 with STAT5 from non-starved MedB-1 cells. Protein markers (kDa) are included. **B**, gel of an immunoprecipitation (IP) of STAT5 from starved MedB-1 cells. Bands where STAT5 and SHP1 were identified by mass spectrometry are indicated. Protein markers (kDa) are shown. **C**, SHP1 protein identification by MASCOT software. Peptides derived from trypsin cleavage (SHP1 band from **B**), are highlighted and cover 51% of SHP1 protein sequence.

Figure S11. Determination of IL4Ra molecules per cell on cell surface

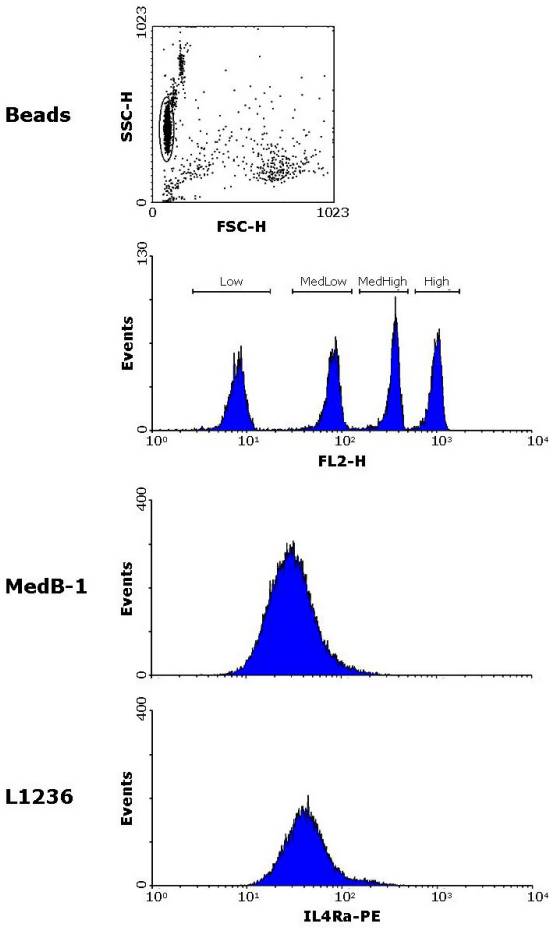

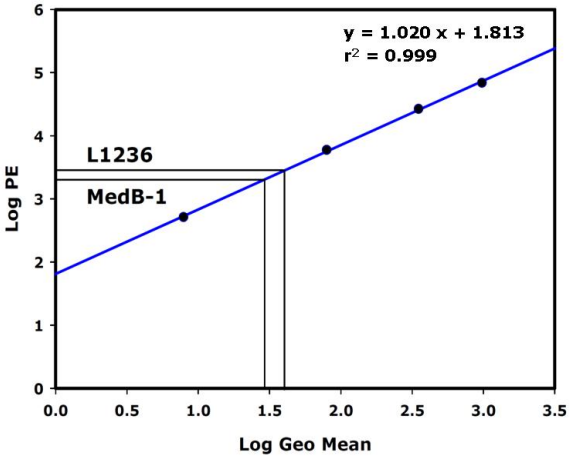

Fig. S11. Quantification of IL4Ra molecules per cell on cell surface. IL4Ra molecules per cell on cell surface were calculated using the QuantiBRITE PE Quantitation kit. Flow cytometric histograms of reference beads, MedB-1 and L1236 cells are provided. The linear regression used for calculation of molecule numbers is included. The estimated values in MedB-1 and L1236 cells are shown (solid black lines).

Figure S12. STAT5, STAT6, SHP1 and JAK2 molecules per cell in MedB-1 cells.

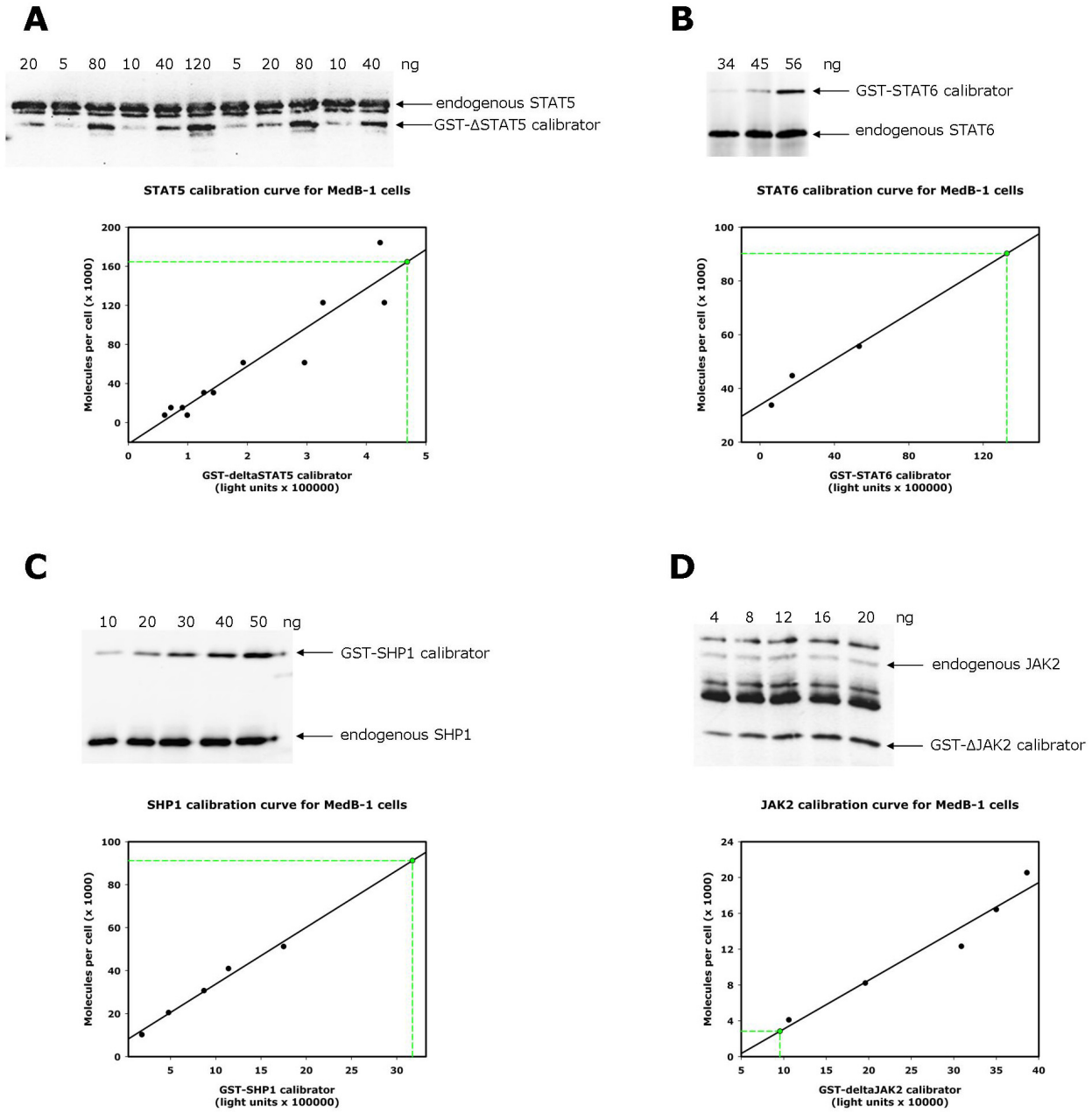

Fig. S12. Determination of molecules per cell of STAT5 (**A**), STAT6 (**B**), SHP1 (**C**) and JAK2 (**D**) in MedB-1 cells. Immunoblots representing the co-IPs of constant amounts of endogenous proteins and dilution series of the corresponding calibrators are shown. A scatter plot of the molecules per cells corresponding to the intensity of each calibrator band is depicted. Band chemiluminescent signal quantification was performed with LumiAnalyst software. Plots include a linear regression of the data points (black line), and the estimated value of molecules per cell of the endogenous protein calculated according to the linear regression (dashes green lines).

Figure S13. STAT5, STAT6, SHP1 and JAK2 molecules per cell in L1236 cells.

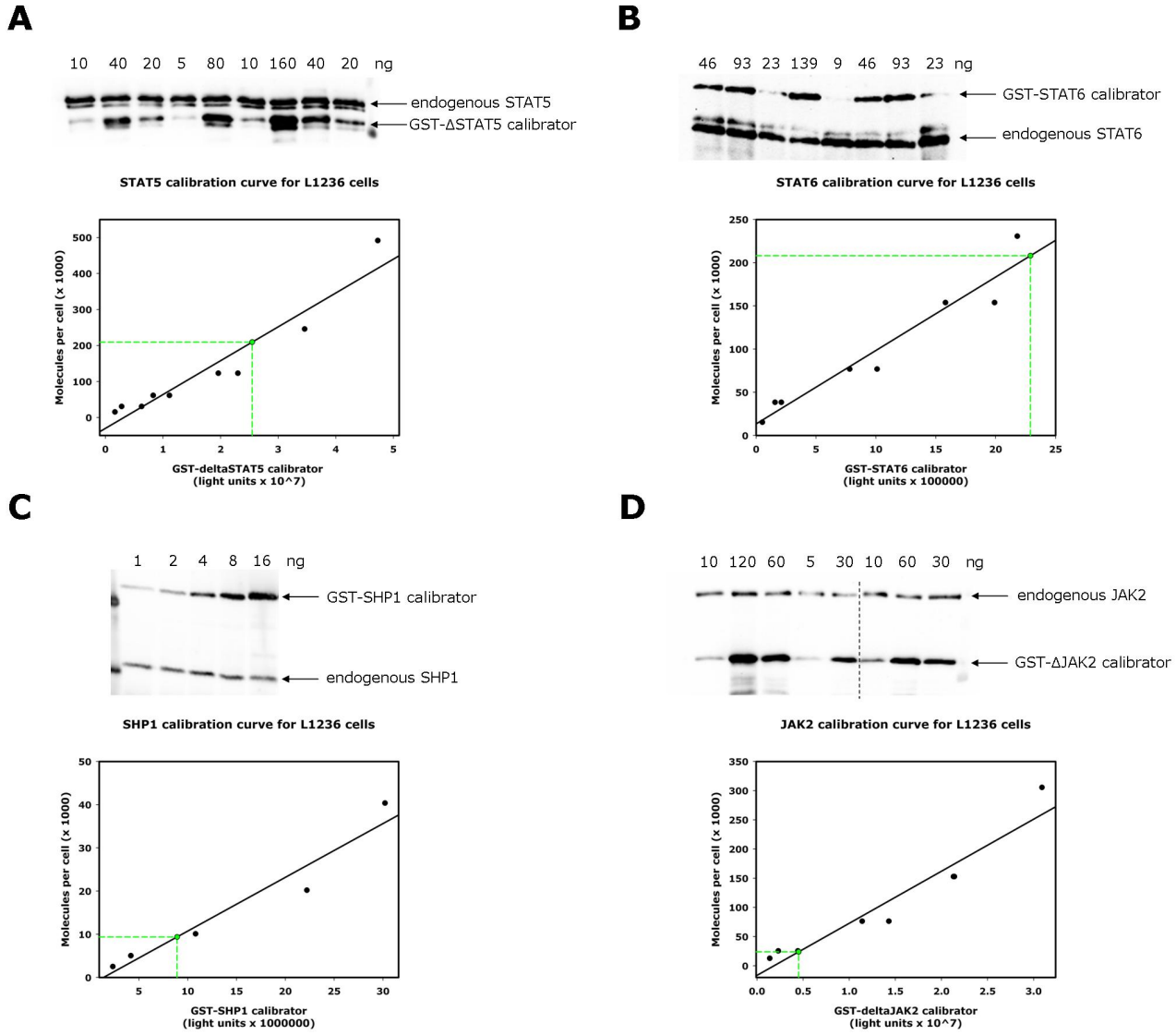

Fig. S13. Determination of molecules per cell of STAT5 (**A**), STAT6 (**B**), SHP1 (**C**) and JAK2 (**D**) in L1236 cells. Immunoblots representing the co-IPs of constant amounts of endogenous proteins and dilution series of the corresponding calibrators are shown. A scatter plot of the molecules per cells corresponding to the intensity of each calibrator band is depicted. Band chemiluminescent signal quantification was performed with LumiAnalyst software. Plots include a linear regression of the data points (black line), and the estimated value of molecules per cell of the endogenous protein calculated according to the linear regression (dashes green lines).

Figure S14. STAT5, STAT6, SHP1 and JAK2 molecules per cell in CD19+ B cells.

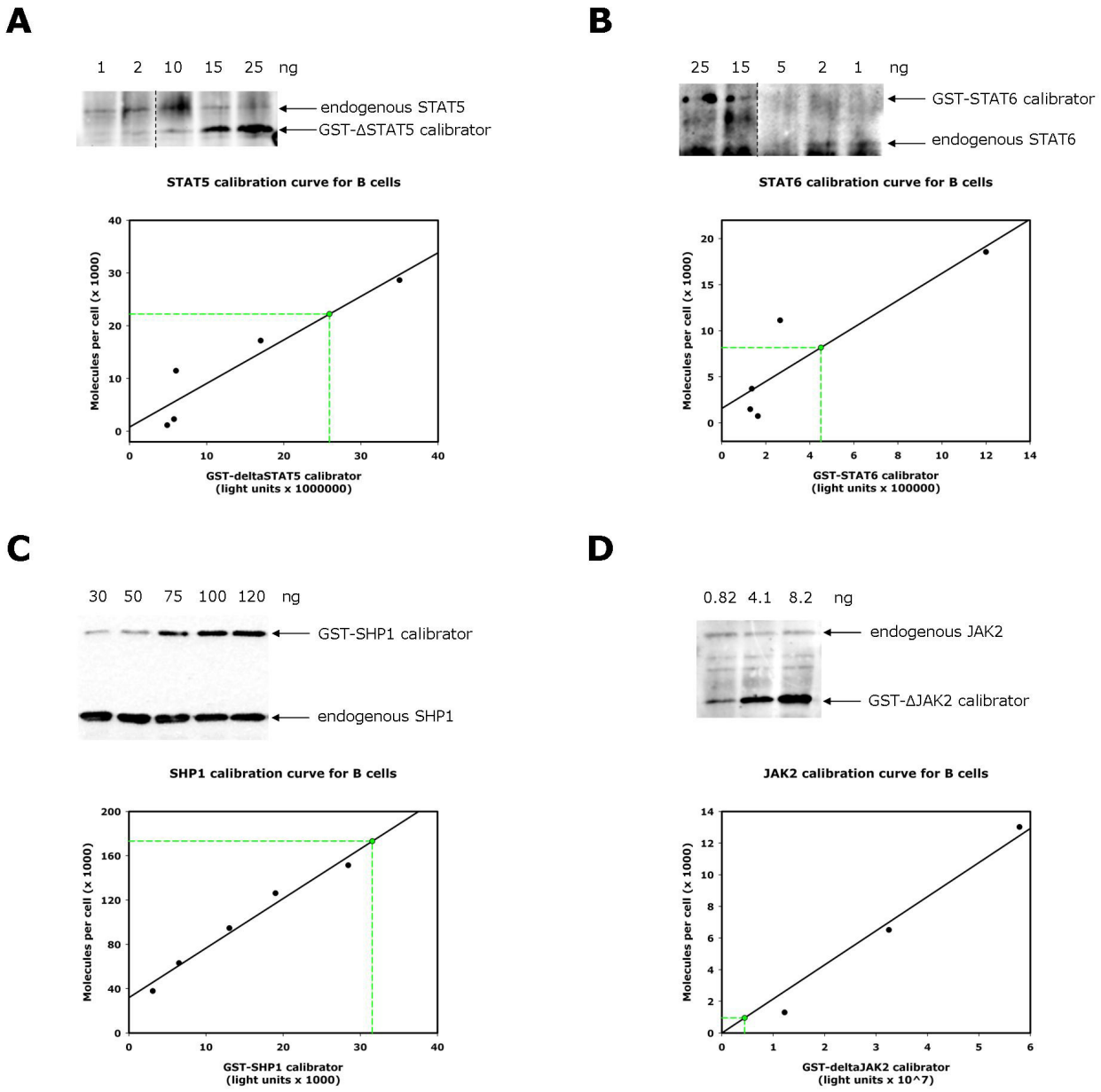

Fig. S14. Determination of molecules per cell of STAT5 (**A**), STAT6 (**B**), SHP1 (**C**) and JAK2 (**D**) in CD19+ B cells. Immunoblots representing the co-IPs of constant amounts of endogenous proteins and dilution series of the corresponding calibrators are shown. A scatter plot of the molecules per cells corresponding to the intensity of each calibrator band is depicted. Band chemiluminescent signal quantification was performed with LumiAnalyst software. Plots include a linear regression of the data points (black line), and the estimated value of molecules per cell of the endogenous protein calculated according to the linear regression (dashes green lines).

Figure S15. Phosphorylation degree analysis of STATs

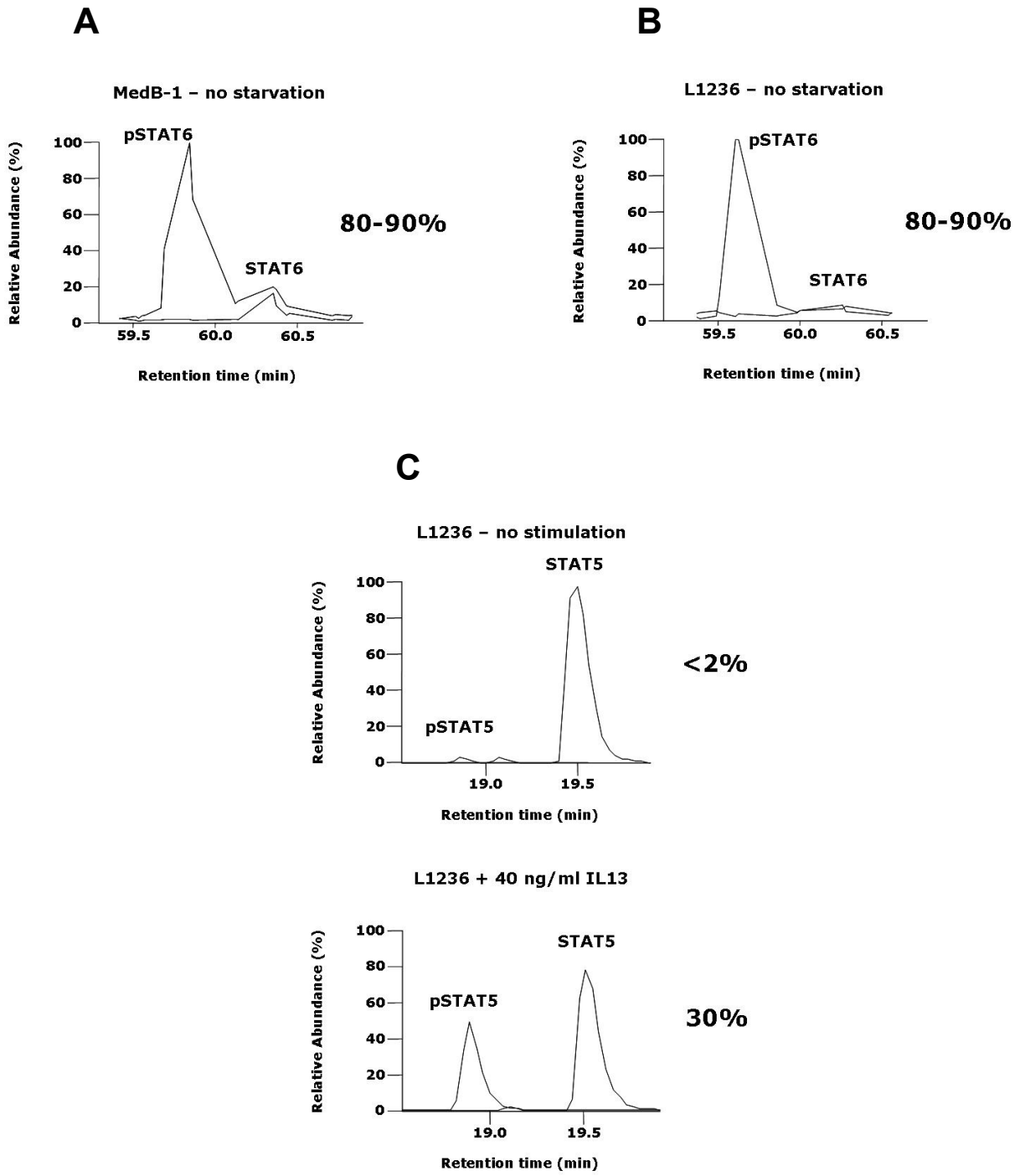

Fig. S15. Measurement of STAT6 phosphorylation degree in MedB-1 (**A**) and L1236 (**B**) cells in normal culture conditions, by mass spectrometric analysis performed in a label-free manner. The results are expressed in percentage of total STAT6. **C**, Measurement of STAT5 phosphorylation degree in starved L1236 cells before and after (40 min) IL13 treatment (40 ng/ml), by mass spectrometric analysis performed with labeled internal peptide/phosphopeptide standards. Chromatograms of endogenous peptides are shown. The results are expressed in percentage of total STAT5.

Figure and table S16. Up-regulated genes in MedB-1 and L1236 cells

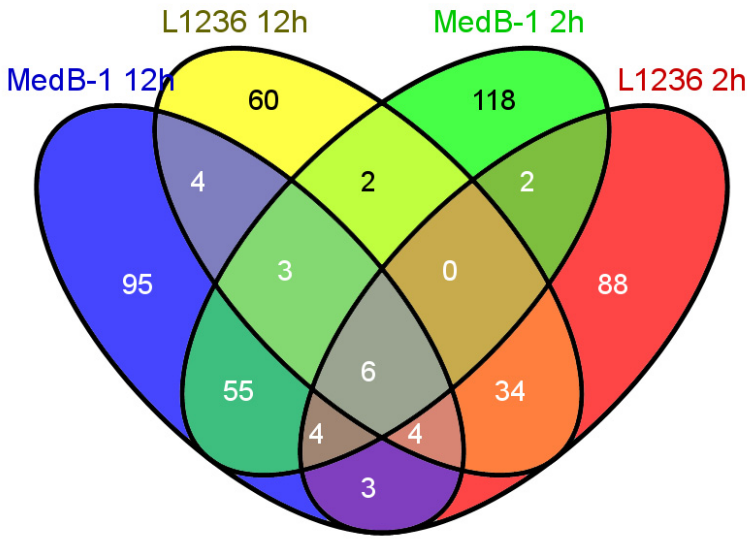

Fig. S16. Venn diagram of IL13-induced genes up-regulated in the early (green ellipse) and sustained (blue ellipse) response in MedB-1 cells and in the early (red ellipse) and sustained (yellow ellipse) response in L1236. Numbers of common genes are in the respective overlapping sections.

Table S16. Table of genes up-regulated following IL13 stimulation

Genes only in the early response in MedB-1	Genes only in the early response in L1236	Genes only in the long-term response in MedB-1	Genes only in the long-term response in L1236	Common genes in early and long-term response in MedB-1	Common genes in early and long-term response in L1236
AADACL3	*AKR1C1*	*ADAP2*	*AANAT*	*ARID3B*	*ARHGAP21*
ADRB2	*ANAPC10*	*AIM1*	*ANK3*	*ARID5A*	*ARPM1*
ADRB3	*ANKRD20B*	*ALPK1*	*ANKRD6*	*B4GALT1*	*C21orf67*
AMELX	*ANXA1*	*ANTXR2*	*ASPN*	*BATF*	*CARD6*
AP1S2	*BAMBI*	*APOL1*	*B3GNT6*	*BCL3*	*CCL2*
BATF2	*BBS12*	*ARAP2*	*BCAR3*	*BHLHE40*	*CCL3L1*
BCL6	*BPESC1*	*ATF3*	*BEST3*	*C10orf10*	*CCNJ*
C10orf78	*C12orf35*	*AUTS2*	*BMPR1B*	*C4orf35*	*CD200R1*
C14orf43	*C15orf29*	*C8orf73*	*BRCA2*	*CD3EAP*	*CD44*
C17orf76	*C1orf124*	*CA5BP*	*C12orf59*	*CXCL10*	*CDC42EP2*
C1orf229	*C5orf20*	*CCDC141*	*C3orf70*	*CXCL9*	*CHML*
C9orf131	*C5orf51*	*CCRN4L*	*CEMP1*	*CXCR5*	*CRISPLD1*
CCDC146	*C6orf224*	*CD80*	*CH25H*	*DUSP5*	*DLEU2*
CCL4	*CCR4*	*CDKN1A*	*CHST11*	*FAM75A7*	*FBXO30*
CD244	*CD209*	*CDRT1*	*CLEC14A*	*FLJ25715*	*FCGR2A*
CD28	*CD79B*	*CHSY1*	*CREG1*	*FLJ36116*	*FLJ44838*
CHRNA10	*CEBPE*	*CMAH*	*CTSC*	*FRMD4B*	*IL6*
CIDECP	*CENPH*	*CP110*	*CXorf64*	*GPR183*	*KMO*
CLDN6	*CNTFR*	*CPEB4*	*DNAI1*	*HAPLN3*	*LRRC8C*
CST1	*COX17*	*CYP21A2*	*DNM1P35*	*HGF*	*MPHOSPH6*
CST7	*CRYGD*	*CYSLTR1*	*EFEMP1*	*ICAM1*	*MYB*
CXCR3	*CST9L*	*CYSLTR2*	*FAM126A*	*ICAM4*	*NKIRAS1*
DEFB130	*CTD-2514C3.1*	*DDIT4*	*FGFBP3*	*IL2RA*	*OR10J5*
DMRT3	*CYP4A22*	*DTX3L*	*FLJ90757*	*IL31*	*PDE4B*
EFCAB4B	*DOC2B*	*ELL2*	*GABPA*	*IL7*	*PELI1*
ENAM	*DUSP6*	*ETV6*	*GAP43*	*IRF1*	*PLK4*
FAM131C	*EPC2*	*EZH2*	*GBX1*	*IRF4*	*PRICKLE2*
FAM48B1	*EVI2B*	*FAM92A2*	*GNAQ*	*JUNB*	*SERPINB2*
FAM48B2	*EXOC5*	*FLJ25758*	*GOLIM4*	*KRT34*	*SNRK*
FLJ20712	*FAM35A*	*FLJ43860*	*GOT1*	*LOC100130713*	*SPRYD5*
FLJ35424	*FEZF2*	*FUT5*	*GPRIN3*	*LOC644714*	*STK17B*
FLJ37396	*FRG1*	*GAD1*	*HADHB*	*LTA*	*TAS2R16*
FOXG1	*GDA*	*GAGE12B*	*HISPPD2A*	*NAMPT*	*TMEM2*
GADD45B	*GDF2*	*GAS7*	*HOXD13*	*OR2A9P*	*TRPC4*
GADL1	*GIMAP1*	*GBP4*	*IGSF3*	*PCDHB8*	
GALNTL1	*GPAM*	*GLRA1*	*LCP2*	*PMAIP1*	
GLI1	*GPR148*	*GLRX*	*LHX9*	*PRDM1*	
H1FNT	*GPR84*	*GPR155*	*LYPD6B*	*PTGER4*	
HBE1	*HIST4H4*	*HLA-DOB*	*NCAPH*	*PTP4A3*	
hCG_2009921	*HMGN1*	*IKZF1*	*NR2F1*	*RGS1*	
HCG27	*INMT*	*IL15RA*	*OR10G7*	*RHOH*	
HOXA11	*ITPRIPL2*	*IRF8*	*PCDH17*	*SIK1*	
HOXD4	*KCNJ2*	*IVNS1ABP*	*PLCL1*	*SLAMF1*	
HTR5A	*KRR1*	*JAK2*	*PRICKLE1*	*SLC45A4*	
IFNA5	*KRT19P2*	*KDSR*	*QSOX1*	*SMAD7*	

Genes only in the early response in MedB-1	Genes only in the early response in L1236	Genes only in the long-term response in MedB-1	Genes only in the long-term response in L1236	Common genes in early and long-term response in MedB-1	Common genes in early and long-term response in L1236
IRS1	*LCMT2*	*KIAA1305*	*REPS2*	*SOCS1*	
ITK	*LOC100132147*	*LACTB*	*ROR2*	*SOCS2*	
KRT1	*LOC389787*	*LAP3*	*SH2D1B*	*SOCS3*	
KRT38	*LOC644717*	*LOC389203*	*SH2D4A*	*STARD5*	
KRT8	*LRTOMT*	*MAP3K5*	*SIGLEC12*	*TAGAP*	
KRTAP10-11	*MBD3L1*	*MAST4*	*SLC16A4*	*THPO*	
KRTAP10-5	*MRPL15*	*MGC23284*	*SPATA13*	*TLR7*	
LCE2B	*MYNN*	*MIRHG2*	*TMEM164*	*TNIP3*	
LELP1	*NEDD9*	*MYBPC2*	*TMEM5*	*TRIM15*	
LHB	*NF1*	*MYEOV*	*TRIM49*	*ZBTB32*	
LOC100008588	*OR2T4*	*NFIL3*	*WDR42B*		
LOC100131642	*PAIP1*	*NFKB1*	*WFS1*		
LOC100131796	*PDCD1LG2*	*NR6A1*	*XG*		
LOC121952	*PLOD2*	*PARP14*	*ZHX2*		
LOC388931	*PSG3*	*PARP9*	*ZRSR1*		
LOC399900	*PTGIR*	*PAX9*			
LOC400804	*PYROXD1*	*PGS1*			
LOC554223	*PYY*	*PIP5K1B*			
LRP3	*RAB1C*	*PRKAB1*			
LY6G5B	*RASGRF2*	*PTGER2*			
LYPD3	*RFC1*	*RBM47*			
MAGEB18	*RNF207*	*RNF19A*			
MGP	*RNF34*	*RRAGD*			
MST150	*RNU4-1*	*SBNO2*			
NCRNA00174	*RPE*	*SEMA6A*			
NPB	*RPL29P15*	*SERPINB1*			
NTN5	*RPL29P8*	*SFXN4*			
NTSR1	*RPRM*	*SLC4A5*			
NUB1	*RPS9*	*SLC7A5*			
NXPH1	*SAMSN1*	*SMAD1*			
OR1G1	*SBK1*	*SOD2*			
OR4A47	*SLITRK6*	*SPIB*			
OR56A4	*SNORD28*	*SSTR2*			
OR5M3	*ST8SIA4*	*STAT3*			
P2RY14	*TFG*	*STAT4*			
PAPPA	*TLR8*	*STAT5A*			
PFN2	*TOM1L1*	*STAT5B*			
PHF5A	*TREX2*	*SYTL3*			
PRF1	*TXNDC9*	*TBC1D13*			
PSAPL1	*ZNF217*	*TNFRSF8*			
RAB42	*ZNF518A*	*TTN*			
RPL13AP3	*ZNF623*	*UNQ6228*			
RPL9	*ZXDB*	*WIPF1*			
RTN4RL2		*ZBTB38*			
RUNDC2C		*ZNF257*			
SBDS		*ZNF259*			
SCHIP1		*ZNF267*			
SERPINB3		*ZNF578*			
SH3BP2		*ZNF676*			
SIX2		*ZNF702P*			
SLC26A5					
SLC7A14					
SLCO4A1					
SLITRK5					
SOX17					
SSX7					
STRC					
SYT15					
TDRG1					
TFF1					
TNXB					
TUBA3E					
UGT2B28					
VSTM2B					
WFDC10B					
XKR4					
ZBED2					
ZBTB42					
ZFP36					
ZNF316					
ZNF350					
ZNF784					
ZNF835					

Table S17. List of common up-regulated genes in MedB-1 and L1236 cells

Common late genes	Common early genes
AMOT	*CD274*
CD274	*GBP1*
CISH	*GCNT2*
FLJ14213	*HSP90AA6P*
GCNT2	*LOC441233*
HSP90AA6P	*MIR21*
LPIN2	*MIRHG1*
MIRHG1	*NUDT4*
MREG	*OR10A2*
NR4A3	*RGS16*
NUDT4P1	*SPIC*
OR10A2	
RGS16	
TNFAIP1	
TP53BP2	
TRAF6	

Figure S18. GraDe analysis

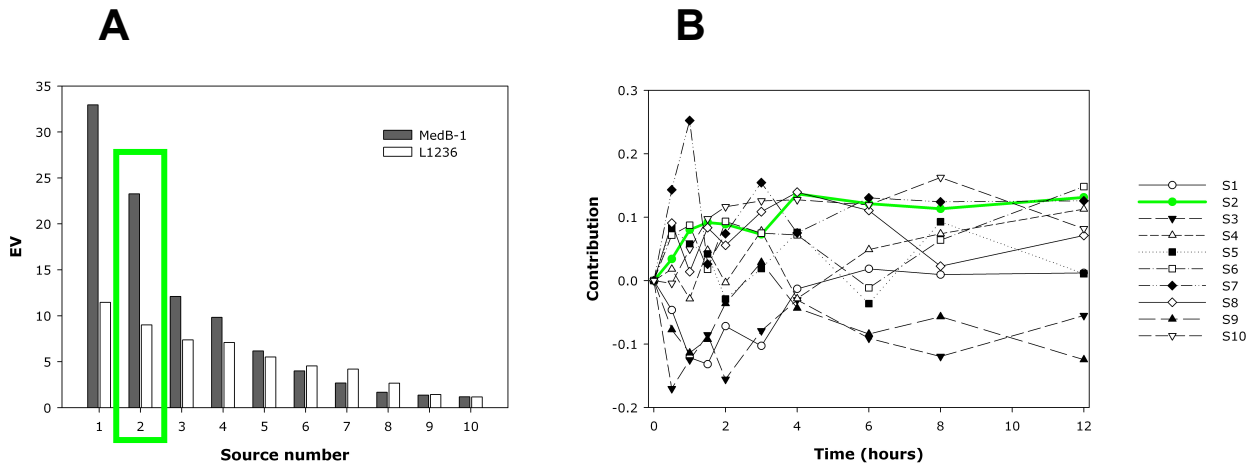

Fig. S18. Results of GraDe. Eigenvalues (EV) in both cell lines (**A**) and time-courses of the sources in MedB-1 cells (**B**). The time-course of source 2 is highlighted in green and shows a strong increase in expression after stimulation followed by a constant high expression level until 12 hours.

Figure S19. Detection of induced SOCS3 protein in MedB-1 cells

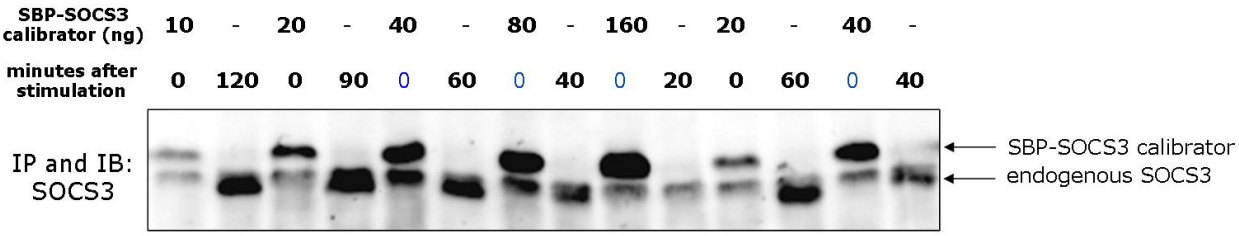

Fig. S19. Detection of induced SOCS3 protein in MedB-1 cells. MedB-1 cells were stimulated with 20 ng/ml IL13 and then lysed at the indicated time points. At time point 0 seven samples (replicates) are taken and immunoprecipitated with known amounts of SBP-SOCS3 recombinant protein. When high amounts of calibrator are added (40, 80 and 160 ng), the endogenous SOCS3 protein seems to be present in higher amounts. Because there is no biological reason for this behavior, we considered this an artifact and thus excluded from the analysis the endogenous bands corresponding to the samples indicated in blue. Only the three samples taken at time point 0 which were not affected by the described artifact were used for quantification.

Figure S20. Measurements of extracellular and cell-associated IL13

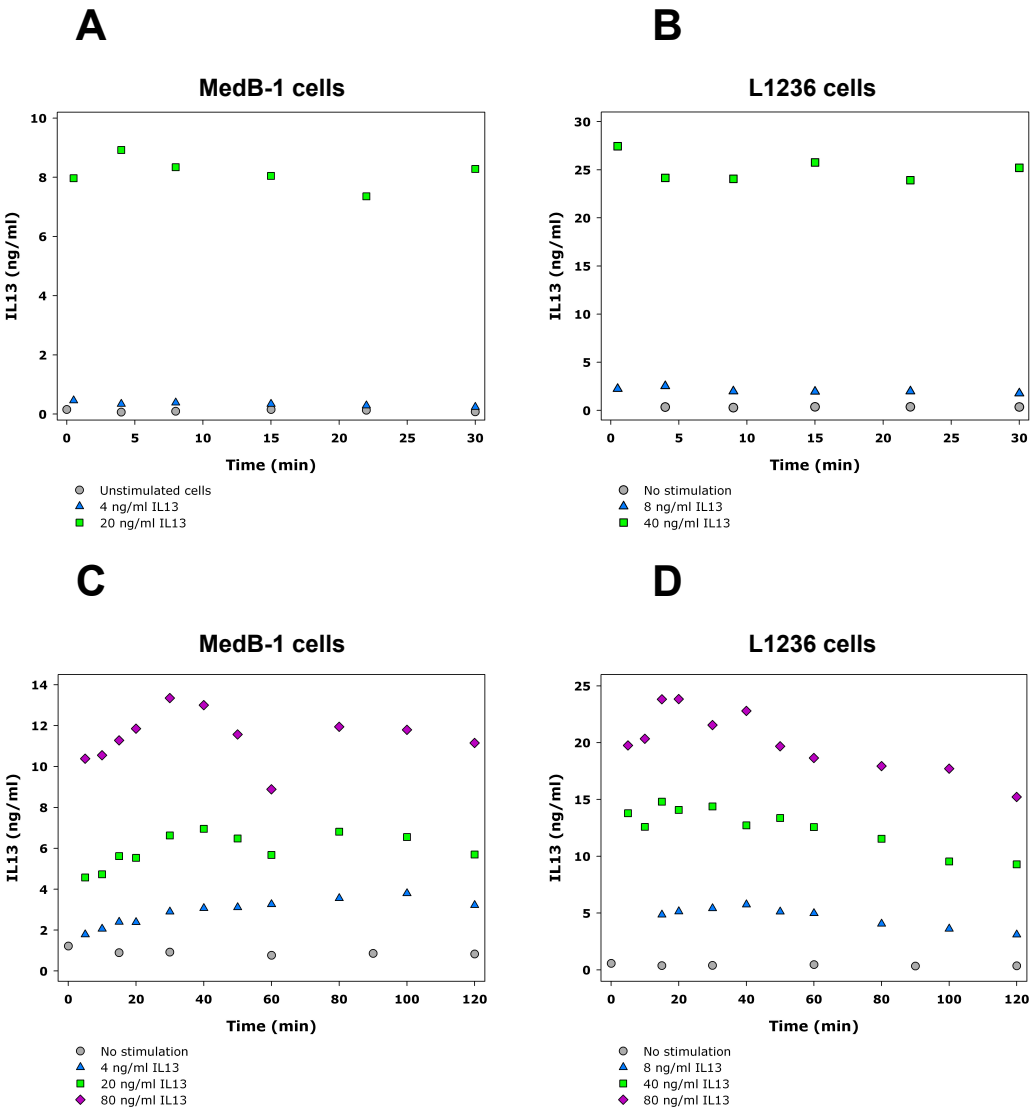

Fig. S20. Measurements of extracellular and cell-associated IL13. IL13 concentration was measured by ELISA over time in the medium of cells stimulated with different concentrations of IL13. Similar results were otained from MedB-1 (**A**) or L1236 (**B**) cells. IL13 taken up by 5 x 10^6 MedB-1 cells (**C**) and 3 x 10^6 L1236 cells (**D**) over time after stimulation with different doses of IL13 was measured. Untreated cells are included as control in each panel. The data shown are the average of two technical duplicates.

Figure S21. Measurements of IL4Ra on cell surface over time

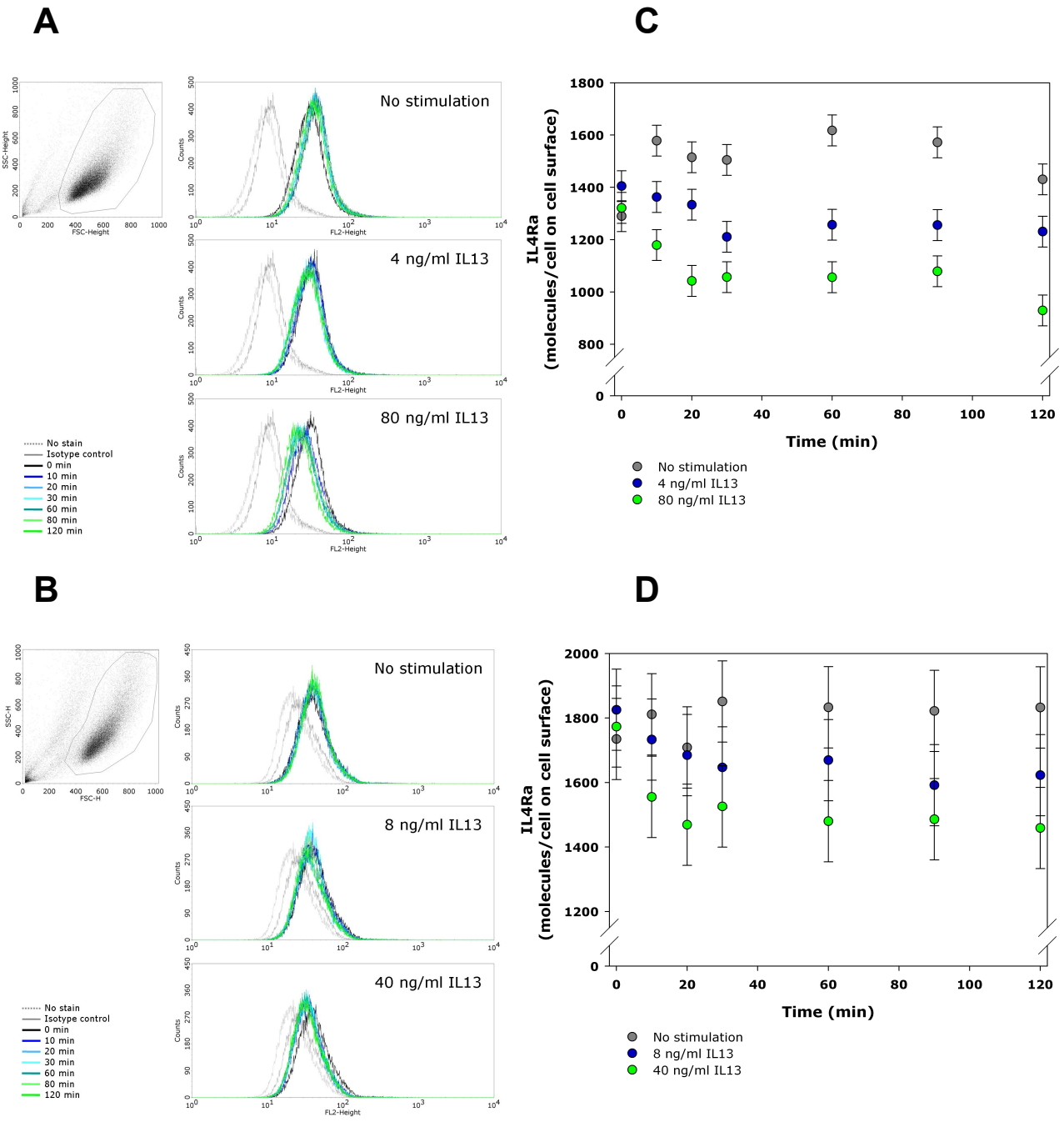

Fig. S21. Measurements of IL4Ra on cell surface over time. **A**, MedB-1 cells treated with 4 or 80 ng/ml IL13 and, **B**, L1236 cells treated with 8 or 40 ng/ml IL13, were analyzed for their surface expression of IL4Ra over time by flow cytometry. Results expressed in molecules per cell on cell surface are shown in panels **C** for MedB-1 cells, and **D** for L1236 cells. The experiment was repeated three times with comparable results. Error bars are error estimations based on the standard deviation of 4 replicate measurements in unstimulated cells (0 minutes).

Figure S22. Kinetics of activation of IL4Ra and JAK2

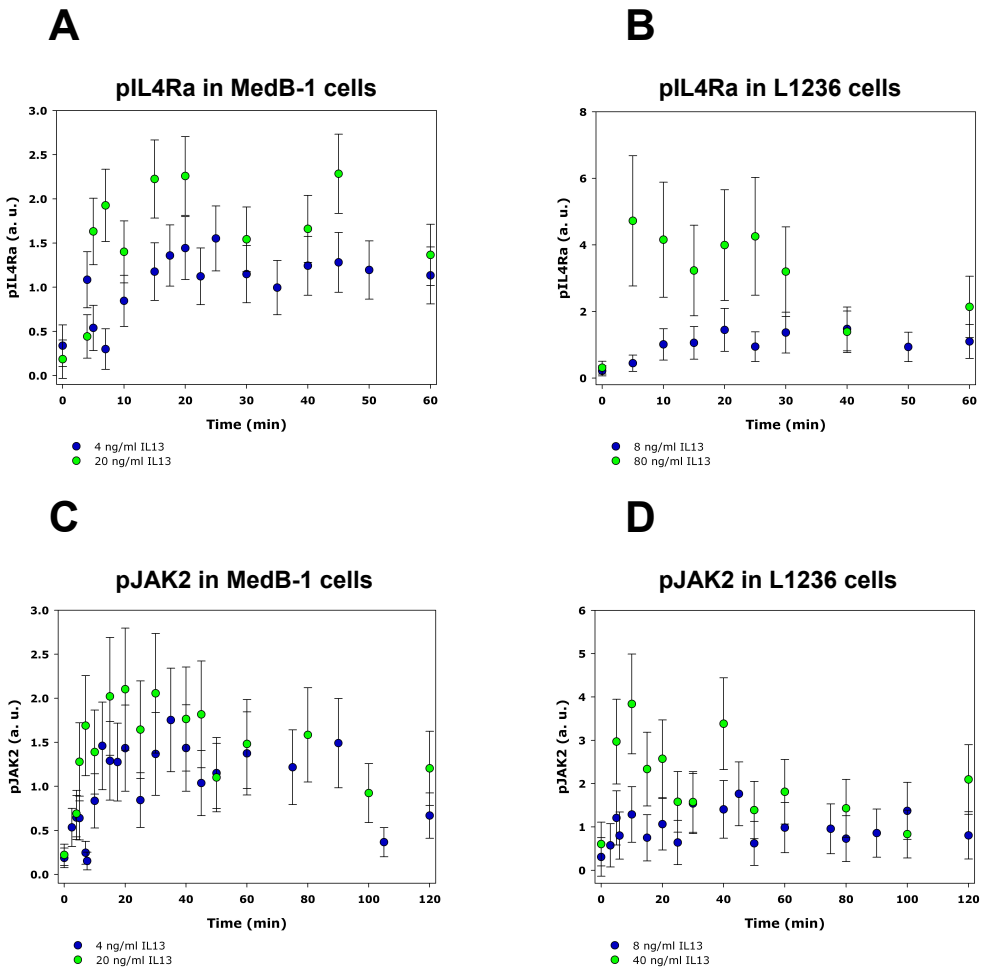

Fig. S22. Kinetics of phosphorylation of IL4Ra and JAK2 monitored by quantitative immunoblotting. Band chemiluminescent signal quantification was performed with LumiAnalyst software. The results obtained from at least three experiments monitoring the activation of IL4Ra (**A**, **B**) and JAK2 (**C**, **D**) upon IL13-stimulation were normalized and merged (**A** and **C**, MedB-1; **B** and **D**, L1236). Error bars are derived from a linear error model (see Supplementary methods S3 for details).

Figure S23. Kinetics of activation of STAT5 in L1236 cells

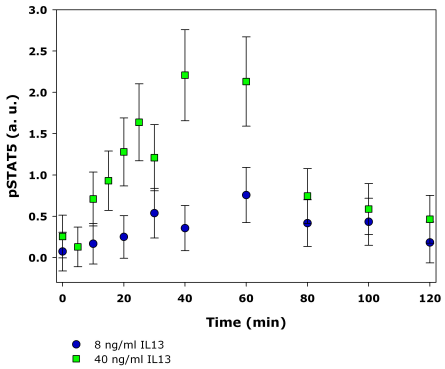

Fig. S23. Kinetics of phosphorylation of STAT5 in L1236 cells monitored by quantitative immunoblotting. Band chemiluminescent signal quantification was performed with LumiAnalyst software. The results derived from three experiments were normalized and merged. Error bars are derived from a linear error model (see Supplementary methods S3 for details).

Figure S24. DecoyR is needed in MedB-1 model

We compared the final MedB-1 model (**Fig. S24A**), with 23 parameters, with the same model without DecoyR (**Fig. S24B**), with 22 parameters, to test whether it is possible to represent the data even with a smaller model. Applying the χ^2 test, both models had a p value >0.01 and could not be rejected, but the χ^2 value of the model with 23 parameters was smaller than the one of the model with 22 parameters (**Fig. S24A-B**). To test whether this smaller χ^2 in the bigger model is statistically significant or just due to a higher number of parameters, we performed a log likelihood ratio test. Based on the resulting p value <0.05 (p=0.0132) of this model comparison, the bigger model is significantly better compared to the smaller one.

A

Final MedB-1 model

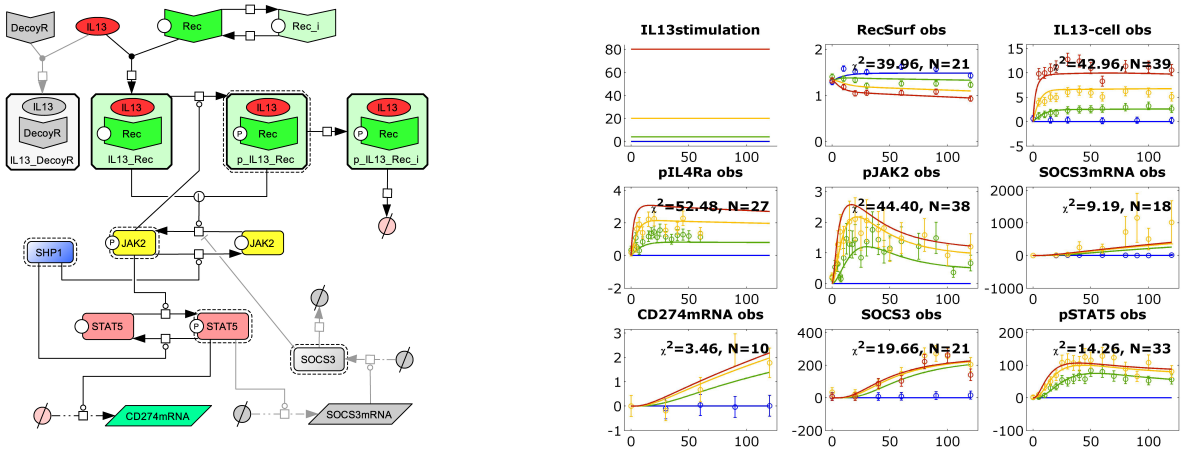

N=207, parameters=23, χ^2=**226.35**, p=0.0182

B

Final MedB-1 model without IL13Ra2 decoy receptor

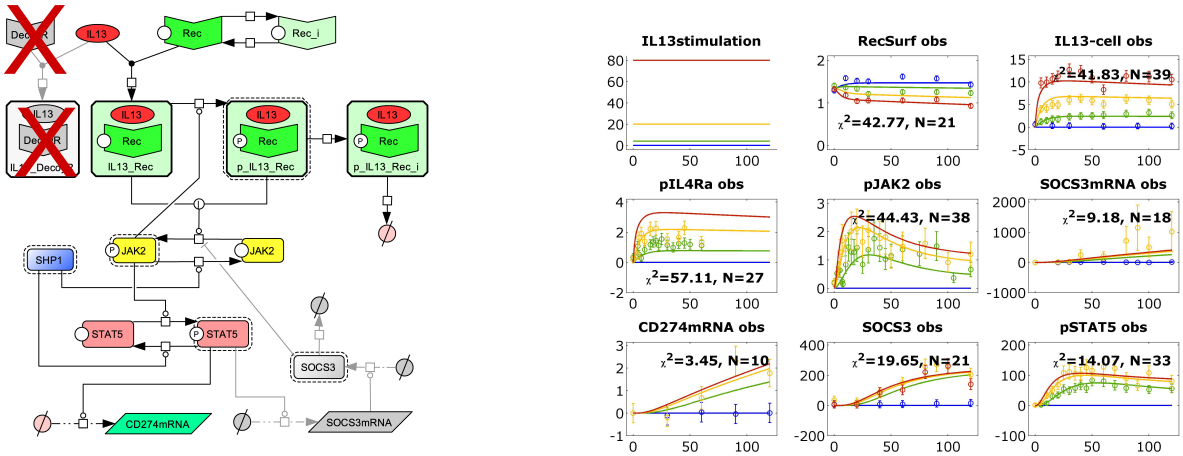

N=207, parameters=22, χ^2=**232.488**, p=0.0102

Fig. S24. Comparison of MedB-1 models with and without DecoyR. **A**, final MedB-1 model - structure and trajectories (best of 1000 parameter estimations). **B**, MedB-1 model like in **A**; but without DecoyR - structure and trajectories (best of 1000 parameter estimations).

Figure S25. Best parameter estimation of L1236 model

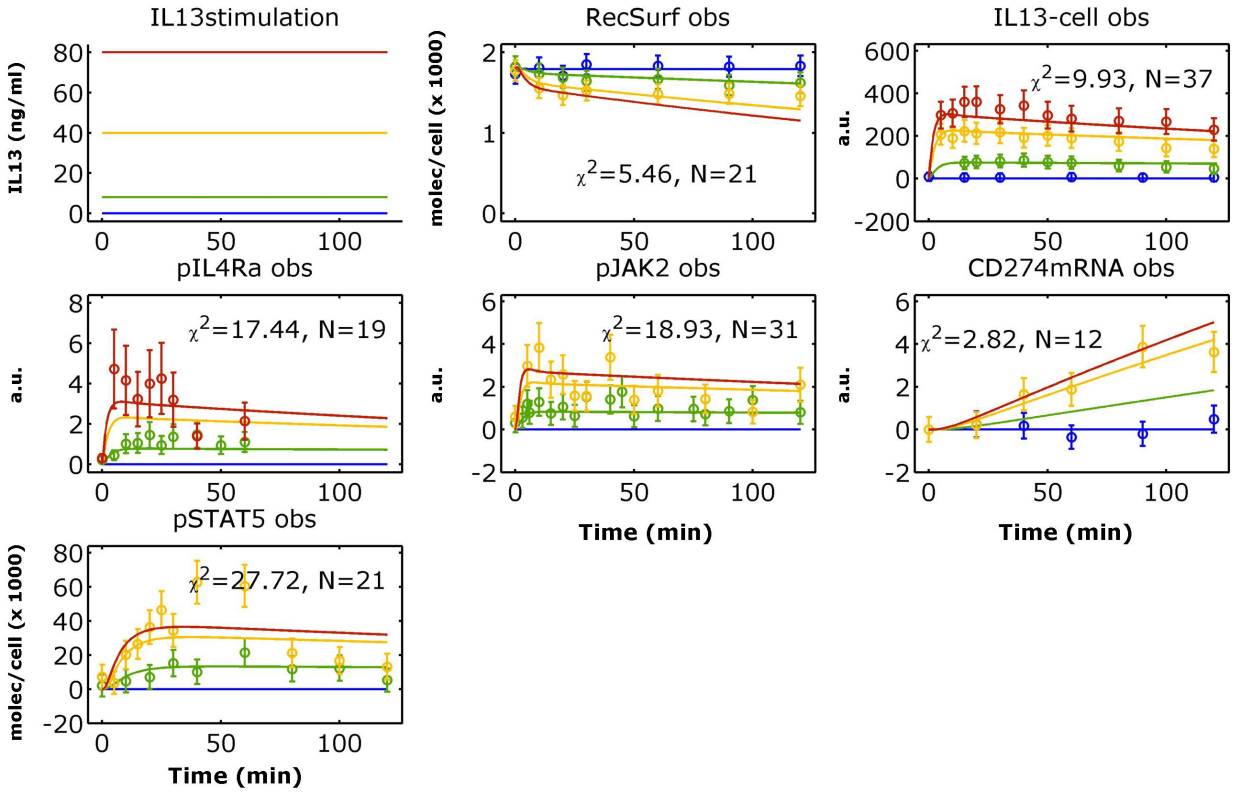

Fig. S25. L1236 mathematical model can represent experimental data. Data (circles) and trajectories of the best L1236 parameter estimation obtained by using the MATLAB® toolbox PottersWheel (obs=observations). Number of data points=141; parameters=16; χ^2=82.30; p>0.01.

Figure S26. Examples of rejected MedB-1 model structures

In mathematical models that consist of differential equations, as in our case, the structure of the equations determines to a large extent how possible trajectories look like (8). Several alternative MedB-1 model structures are conceivable and were therefore tested in **Fig. S26**, but were rejected because they did not sufficiently represent the experimental data, meaning that according to the χ^2 test their p-value was <0.01. In **Fig. S26A** the model structure does not comprise potential receptor recycling or degradation of the phosphorylated receptor, but it considers both reactions Kon_IL13Rec and Rec_phosphorylation as reversible. Moreover, phosphorylation of JAK2 by IL13_Rec and p_IL13_Rec is allowed to occur with two different reaction velocities, instead of just one triggered by either of the two molecules, as represented in our final MedB-1 model (**Fig. 4A**). Additionally, based on the assumption that STAT5 can be phosphorylated by pJAK2 if recruited to the cell membrane by the phosphorylated tyrosine residue on the receptor, the reaction of phosphorylation of STAT5 is triggered only when both pJAK2 and p_IL13_Rec are present. On the contrary in our final MedB-1 model, in order to have a pJAK2-triggered phosphorylation of STAT5, it is not necessary for the receptor to be phosphorylated, too. This might be due to the high number of STAT5 molecules per cells in the studied lymphoma cells. Finally, no gene expression is included in the model. As shown in **Fig. S26** right panels, this model cannot reproduce the experimental data. Likewise, the model displayed in **Fig. S26B** containing, in addition to the reactions in **Fig. S26A**, gene expression and SOCS3 negative regulation, is not suitable to represent the experimental data. Furthermore, as demonstrated in **Fig. S26C**, removing receptor recycling from our final MedB-1 model structure causes a dramatic drop in the goodness-of-fit. In addition without DecoyR and without the degradation reaction of the internalized phospho-receptor, the p-value of the best of 1000 parameter estimations is too low for model acceptance (**Fig. S26D**).

A

Reversible reactions at the receptor level, different JAK2 and STAT5 phosphorylation reactions and no negative feedback

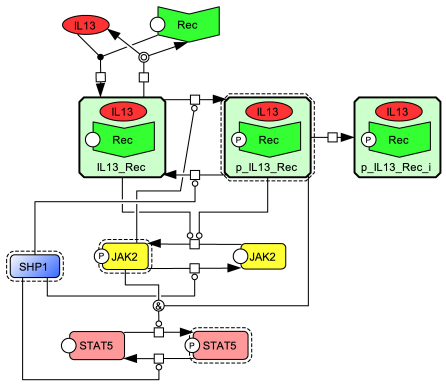

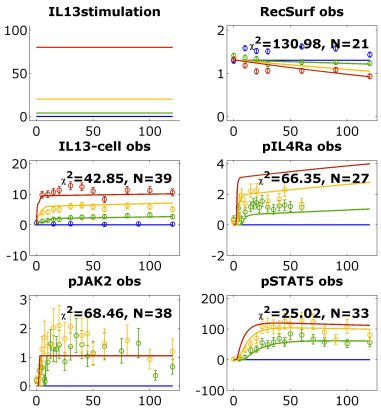

N=158, parameters=13, χ^2=**333.65**, p<<0.01

B

Reversible reactions at the receptor level, different JAK2 and STAT5 phosphorylation reactions, gene expression and SOCS3 negative feedback

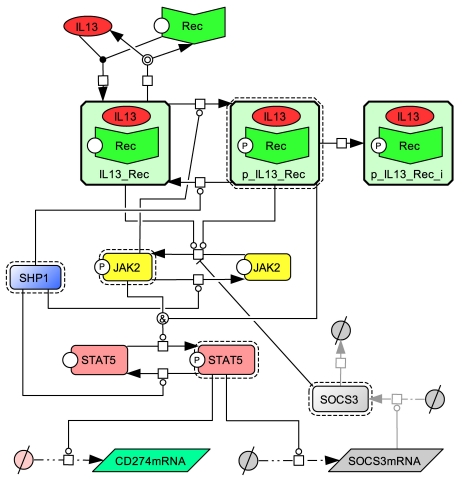

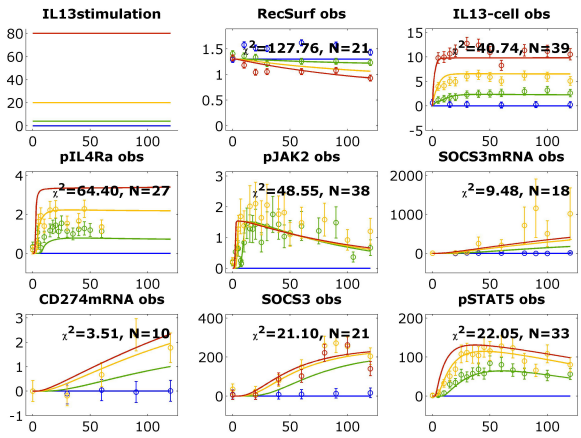

N=207, parameters=22, χ^2=**337.59**, p<<0.01

C

Irreversible receptor reactions, absence of receptor recycle

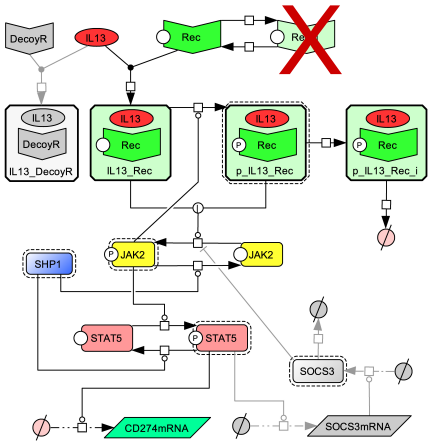

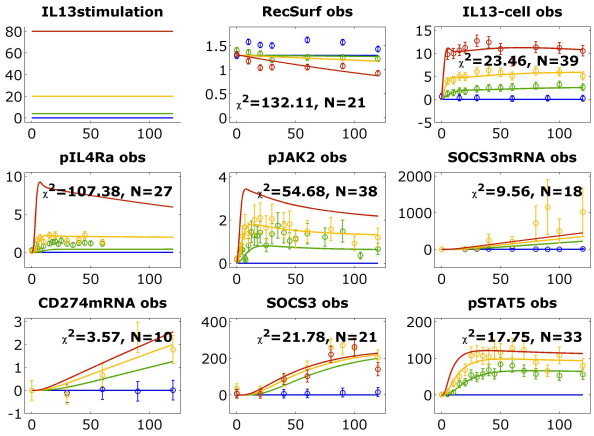

N=207, parameters=20, χ^2=**370.29**, p<<0.01

D

Irreversible receptor reactions, absence of decoy receptor, absence of receptor degradation, presence of receptor recycle

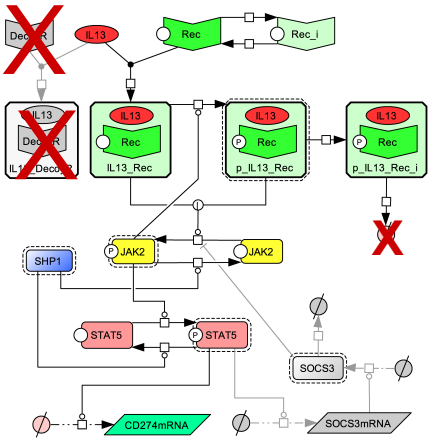

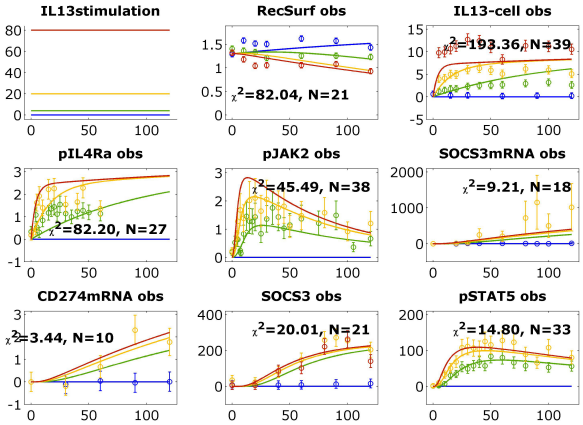

N=207, parameters=21, χ^2=**450.56**, p<<0.01

Fig. S26. Model structures that do not represent the data. **A**, MedB-1 model structure and trajectories (best of 1000 parameter estimations) where Kon_IL13Rec and Rec_phosphorylation reactions are reversible, IL13_Rec and p_IL13_Rec trigger JAK2_phosphorylation via two independent reactions and STAT5_phosphorylation is triggered when both pJAK2 and p_IL13_Rec are present. **B**, model like in **A**, but with *CD274* and *SOCS3* gene expression and SOCS3 negative regulation. **C**, final MedB-1 model without receptor recycle. **D**, final MedB-1 model without DecoyR and without degradation of the internalized phosphorylated receptor.

Figure S27. Structural identifiability analysis for the L1236 model

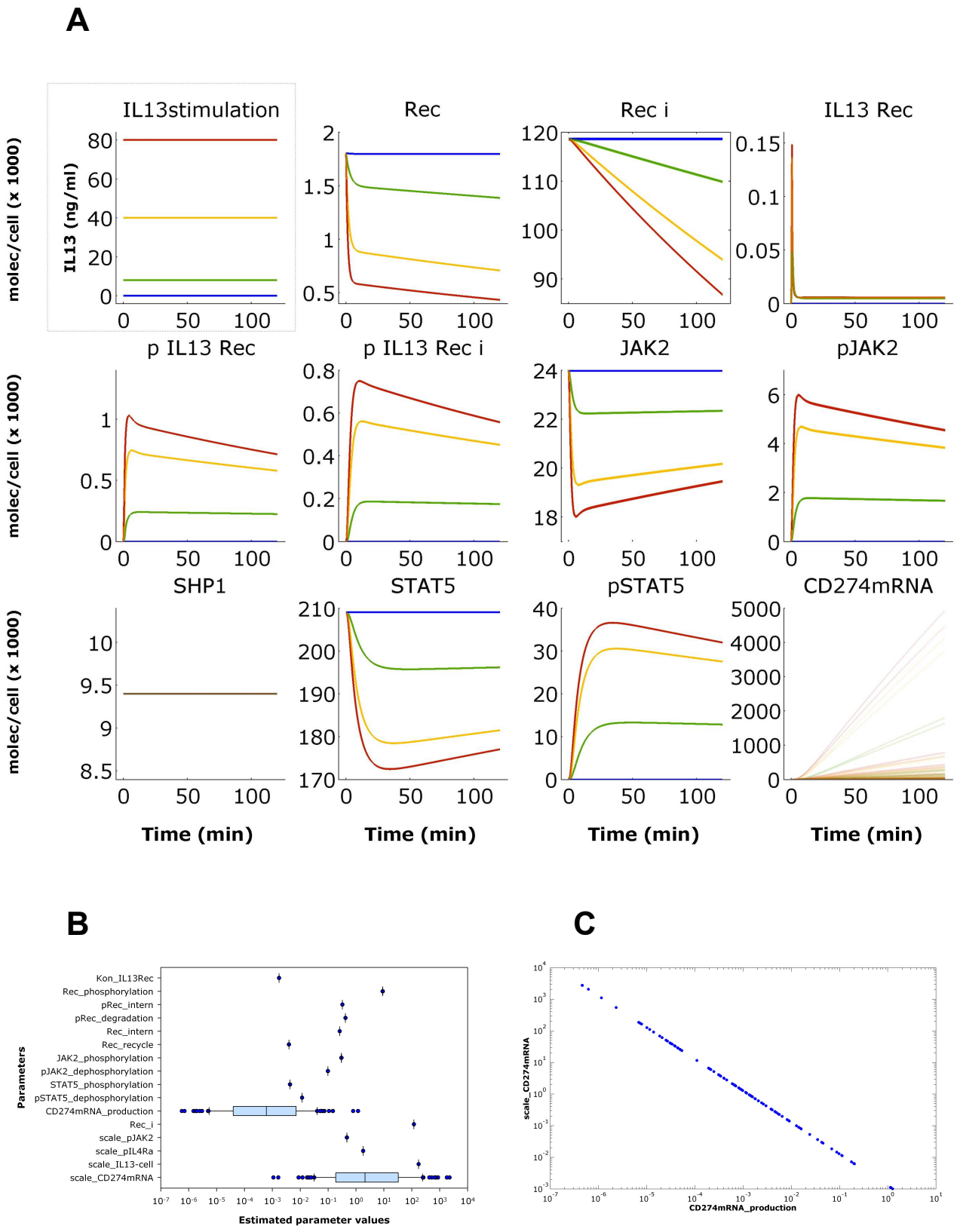

Fig. S27. Structural identifiability analysis of the L1236 model. Trajectories (**A**) and parameter distribution, highlighting the non-identifiable parameters (larger boxes), (**B**) of 10% best of 1000 parameter estimations. Relation of the two CD274-associated (**C**) parameters. The MATLAB® toolbox PottersWheel was used for this analysis.

Figure S28. L1236 model validation

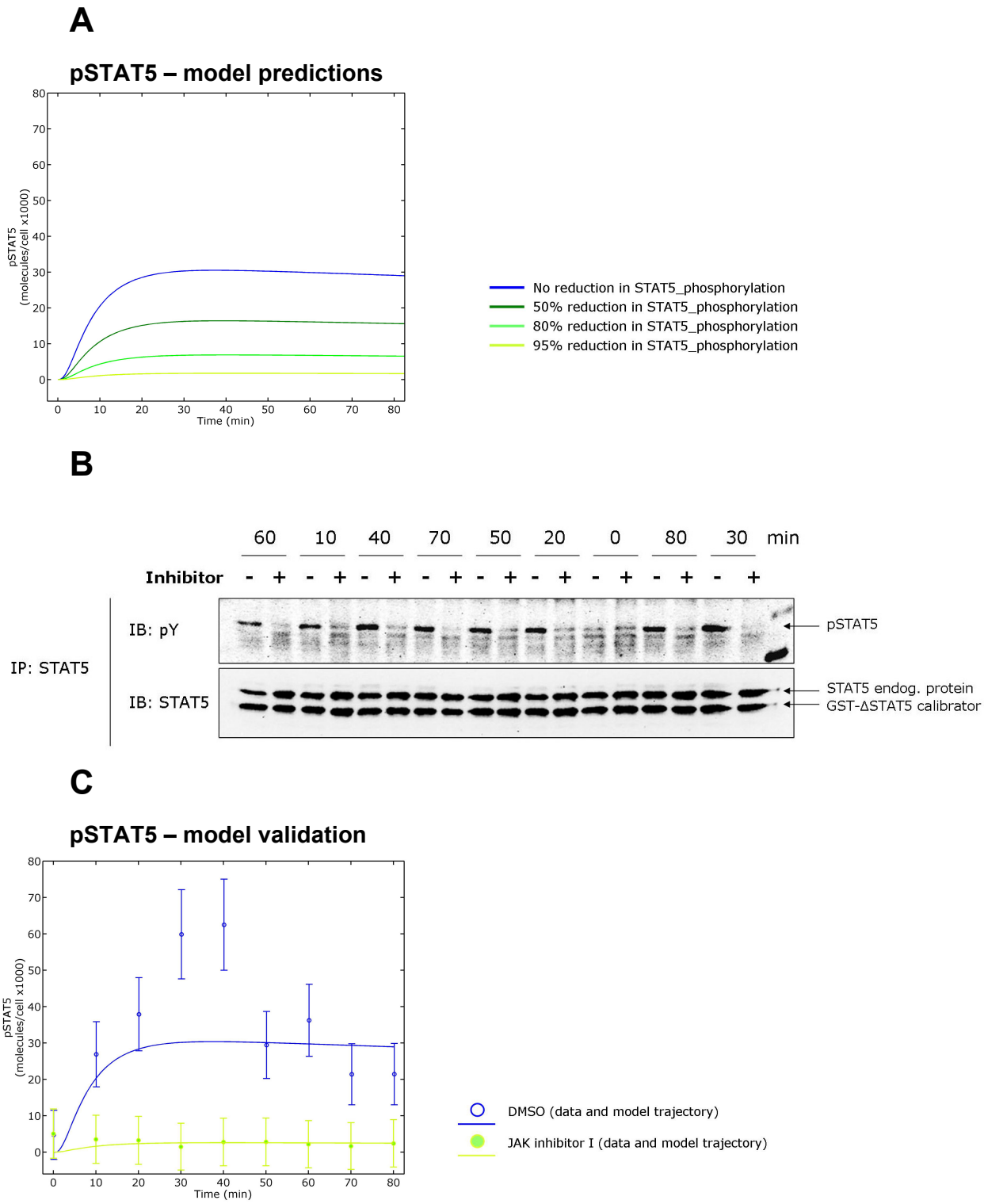

Fig. S28. L1236 model predictions and validation. **A**, prediction of the effect on pSTAT5 of 50%, 80% and 95% reduction of STAT5_phosphorylation parameter. Immunoblotting evidence of pSTAT5 reduction upon 160 nM JAK inhibitor I treatment (1 hour pre-incubation followed by 40 ng/ml IL13 stimulation) (**B**) and graphic representation of the results. Chemiluminescent band signal quantification was performed with LumiAnalyst software (**C**). Error bars are derived from a linear error model (see Supplementary methods S3 for details). Experiment was repeated 3 times with comparable results.

Supplementary references

1. Vera J, Bachmann J, Pfeifer AC*, et al.* A systems biology approach to analyse amplification in the JAK2-STAT5 signalling pathway. BMC Syst Biol 2008;2:38.
2. Schilling M, Maiwald T, Bohl S*, et al.* Quantitative data generation for systems biology: the impact of randomisation, calibrators and normalisers. Syst Biol (Stevenage) 2005;152(4):193-200.
3. Schilling M, Maiwald T, Hengl S*, et al.* Theoretical and experimental analysis links isoform-specific ERK signalling to cell fate decisions. Mol Syst Biol 2009;5:334.
4. Schilling M, Maiwald T, Bohl S*, et al.* Computational processing and error reduction strategies for standardized quantitative data in biological networks. FEBS J 2005;272(24):6400-11.
5. Sanger F, Nicklen S, Coulson AR. DNA sequencing with chain-terminating inhibitors. Proc Natl Acad Sci U S A 1977;74(12):5463-7.
6. Blöchl F, Kowarsch A, Theis FJ. Second-order source separation based on prior knowledge realized in a graph model. LVA/ICA 2010: LNCS 6365; 2010. p. 434-41.
7. Krull M, Pistor S, Voss N*, et al.* TRANSPATH: an information resource for storing and visualizing signaling pathways and their pathological aberrations. Nucleic Acids Res 2006;34(Database issue):D546-51.
8. Rand DA, Shulgin BV, Salazar D, Millar AJ. Design principles underlying circadian clocks. J R Soc Interface 2004;1(1):119-30.